THE ASTRONOMICAL JOURNAL, 122:3317–3324, 2001 December

THE OPTICAL PROPER MOTIONS OF HH 7–11 AND CEPHEUS E

ALBERTO NORIEGA-CRESPO
SIRTF Science Center, California Institute of Technology, IPAC 100-22, Pasadena, CA 91125; alberto@ipac.caltech.edu
AND
PETER M. GARNAVICH
University of Notre Dame, Nieuwland Science Hall 213, Notre Dame, IN 46556; pgarnavi@nd.edu
Received 2001 May 29; accepted 2001 September 20

ABSTRACT

A key ingredient in understanding the dynamics of stellar outflows is their proper motion. We have used optical images in the [S II] emission at 6717/6731 Å and the red Digitized Palomar Observatory Sky Survey (DSS) plates to determine the proper motion of the HH 7–11 system and the optical knot of Cep E (HH 377). The DSS plate measurements span nearly 37 years for both HH 7–11 and HH 377 and have a wide field of view, which allows an accurate determination of the proper motions despite their relatively low angular resolution. The optical images, with higher angular resolution, cover a shorter period, 7 and 4 years, respectively, for HH 7–11 and HH 377 and have been used to complement the DSS measurements. From the DSS plates we have found that HH 377 has a proper motion of $0\farcs031 \pm 0\farcs003$ yr^{-1} with P.A. = 206°; i.e., it is moving away from IRAS 230111+63, which at a distance of 730 pc corresponds to a tangential velocity of 107 ± 14 km s^{-1}. The values obtained from the optical images are consistent with these measurements. Similarly, the proper motions of HH 7–11 range from $0\farcs015 \pm 0\farcs009$ yr^{-1} (HH 9) to $0\farcs044 \pm 0\farcs007$ yr^{-1} (HH 11), and the flow is moving away from SVS 13 with mean P.A. ~ 136°. At a distance of 330 pc, these motions correspond to tangential velocities of ~25–70 km s^{-1}, i.e., comparable to the original values obtained by Herbig & Jones (1983). The measurements from the optical CCD [S II] images are again consistent with these motions, although in detail there are some differences, particularly for HH 7 and HH 10.

Key words: ISM: Herbig-Haro objects — ISM: jets and outflows — ISM: kinematics and dynamics — stars: winds, outflows

1. INTRODUCTION

It has been nearly 20 years since the association between Herbig-Haro objects and bipolar jets from newly formed stars was established. A fundamental element for this conclusion was the determination of the proper motions of the HH 1/2 system, which showed atomic or ionic gas moving away in opposite directions from an embedded source at flow velocities of ~300–450 km s^{-1} (Herbig & Jones 1981; Pravdo et al. 1985). The fact that large-format CCDs with small pixels have been around for almost a decade has made it possible to measure relative proper motions more accurately, replacing the photographic methods. These relative proper-motion measurements have been particularly successful for nearby Herbig-Haro outflows, where flow velocities of ~100–400 km s^{-1} can produce measurable pixel shifts within 4–5 years for an object at a distance of ~150–450 pc, i.e., the distances to the Taurus and Orion molecular clouds, respectively. The method can be applied also on shorter timescales using high angular resolution *Hubble Space Telescope* images, as has been the case for HH 30 (Burrows et al. 1996) and HH 111 (Hartigan et al. 2001).

The results obtained by this method for objects such as HH 1/2 (Eislöffel, Mundt, & Böhm 1994), HH 32 (Curiel et al. 1997), HH 34 (Eislöffel & Mundt 1992; Heathcote & Reipurth 1992; Devine et al. 1997), HH 46–47 (Eislöffel & Mundt 1994), and HH 110/111 (Reipurth, Raga, & Heathcote 1992, 1996) among others, have provided a unique picture of the dynamical behavior of these outflows. High angular resolution radio observations based on the same principle have confirmed some of these results (e.g., for HH 1/2; Rodríguez et al. 1990) and given new measurements for systems such as HH 80–81 (Martí, Rodríguez, & Reipurth 1998). The method is now being used in the near-infrared, thanks to large-format infrared arrays that allow covering wider fields of view and including more reference stars. Objects such as HH 1/2 (Noriega-Crespo et al. 1997), HH 46/47 (Micono et al. 1998), GGD 37 (Raines et al. 2000), HH 7–11 and HH 25/26 (Chrysostomou et al. 2000), and OMC-1 (Lee & Burton 2000) have proper motions measured either in H_2 2.12 μm or [Fe II] 1.67 μm. Nevertheless, we believe that in some cases the smaller field of view and shorter time baseline provided by the IR arrays make some of these results less conclusive than optical measurements.

The present work is motivated precisely by the difference between the optical and the near-infrared measurements of the proper motions of HH 7–11. The tangential flow velocities of the atomic or ionic gas inferred by using the photographic plate method are ~20–60 km s^{-1} (Herbig & Jones 1983), while those of the molecular gas (H_2), determined by using the near-infrared imaging method, are ~300–400 km s^{-1} (Chrysostomou et al. 2000). This difference is difficult to explain from the theoretical point of view, since in other systems we observe quite similar velocities for both gas components (Noriega-Crespo et al. 1997; Micono et al. 1998). In the case of HH 7–11, the driving source, SVS 13, is a relatively low mass protostellar object, which makes it even harder to explain the large H_2 proper motions (see § 4). Another goal of this project is to measure the proper motions of semiembedded outflows. This is the case for HH 7–11, where the counterflow is nearly invisible, and Cep E (HH 377), where most of the outflow is invisible at optical wavelengths (Ayala et al. 2000).

TABLE 1

HH 7–11 AND CEPHEUS E (HH 377) DATA

Date	Band	Scale (arcsec pixel^{-1})	Telescope
HH 7–11:			
1955 Oct 24	DSS E red	1.70	Palomar 48 inch Schmidt
1992 Sep 30	DSS II red IIIa-F	1.00	Palomar 48 inch Schmidt
1993 Oct 12	[S II] λλ6717/6731	0.65	Mt. Hopkins 1.2 m
2000 Nov 29.....	[S II] λλ6717/6731	0.40	VATT
Cep E:			
1953 Oct 31	DSS E red	1.70	Palomar 48 inch Schmidt
1991 Sep 3.....	DSS II red IIIa-F	1.00	Palomar 48 inch Schmidt
1996 Sep 16	[S II] λλ6717/6731	0.65	Mt. Hopkins 1.2 m
2000 Nov 30.....	[S II] λλ6717/6731	0.40	VATT

In this study we determine the proper motions of HH 7–11 and Cep E (HH 377), using digitized plates and optical CCD images. Both outflows are clearly seen in the Digitized Palomar Observatory Sky Survey (DSS), first and second generation, and they provide a time baseline of nearly 37 years. The CCD images cover a period of 7 and 4 years, respectively, for HH 7–11 and HH 377, with the most recent images taken on 2000 November 30 (see below).

2. OBSERVATIONS

The optical images were obtained with the Fred L. Whipple (FLWO) 1.2 m telescope and AndyCam CCD camera on 1993 October 12 (HH 7–11) and 1996 September 16 (Cep E). A narrowband filter centered at 672.5 nm with width 3.0 nm (FWHM) was used to isolate the [S II] emission. Second-epoch images were taken with the 1.8 m Vatican Advanced Technology Telescope (VATT) and VATTCCD camera on 2000 November 30. A similar narrow filter centered at 672.3 nm with width 3.5 nm was employed at the VATT. In all cases the CCD was binned by 2 in both directions, providing an effective scale of 0.″63 pixel^{-1} at FLWO and 0.″40 pixel^{-1} at the VATT.

The digitized images were downloaded from the STScI Digitized Sky Survey.[1] We found that both HH 7–11 and Cep E (HH 377) appear in the First Generation Survey, as well as in the Second Generation (Red) Survey. The details of the digitized plates and the ground-based observations are presented in Table 1.

3. ANALYSIS

One needs to be careful when comparing photographic plates with CCD images. We selected the DSS plates as the primary reference because of their long-time baseline, which allows a more accurate measurement of the small pixel shifts produced by the proper motions. The CCD images by themselves cover a period of only 7 years for HH 7–11 and 4 years for HH 377, and so we use them as secondary indicators. The idea is to set the measurements of the CCD images in the same scale of the plates and then check for consistency and/or differences between them. The reason to proceed in this way is to minimize systematic effects that could arise from comparing the different bandpasses used in the plates and the CCD images. The digitized plates are sensitive to radiation similar to that passing through a broadband *R* filter, and so for shock-excited regions, such as those in outflows, this means that they might include emission from collisionally excited lines such as [N II] and [O I] (so not only [S II]), as well as Hα recombination emission, which could spatially arise from very different regions.

Thus, all the CCD images and the second-epoch digitized plates were mapped into the DSS I plate scale of 1.″7 pixel and brought into the same reference system by using 15 stars common to all the images for HH 7–11 and 10 for Cep E. This transformation was performed using the IRAF tasks GEOMAP and GEOTRAN, which take into account relative translations, rotations, and magnifications between images. The selected reference stars do not show any indication of systematic motions, i.e., large radial velocities or proper motions, according to the data derived from SIMBAD and other sources (e.g., Aspin, Sandell, & Russell 2000; Strom, Vrba, & Strom 1976). The selected stars for HH 7–11 and Cep E (HH 377) are shown in Figures 1 and 2, respectively. As in our previous projects (López et al. 1998; Noriega-Crespo et al. 1997; Reipurth et al. 1993), the proper motions were obtained by using a cross-correlation technique over small sections of a pair of images and checked again by measuring the difference between centroids determined by fitting two-dimensional Gaussians. The uncertainty in the measurement of well-resolved bright knots is ~0.1 pixels, in the pixel scale of the reference frame. Although the cross-correlation technique is quite reliable, we are limited by the available knots or structure of the earliest DSS digitized images. Because of this we concentrated on the brightest knots of the HH 7–11 system, despite the fact that the most recent CCD images show a more rich and complex structure. In the case of Cep E, despite its complex structure in the near-infrared, only a knot from the southern lobe is optically visible (Noriega-Crespo 1997; Devine, Reipurth, & Bally 1997).

The difference between pixels as a function of epoch for the HH 7–11 knots and for Cep E (HH 377) are shown in Figures 3 and 5, respectively. The fits to these data are presented in Table 2 and correspond to the squares (Figs. 3 and 5).

4. RESULTS AND DISCUSSION

4.1. *HH 7–11 System*

The proper motions of the HH 7–11 outflow range from 0.″015 ± 0.″009 yr^{-1} (HH 9) to 0.″044 ± 0.″007 yr^{-1} (HH 11),

[1] See http://stdatu.stsci.edu/dss/.

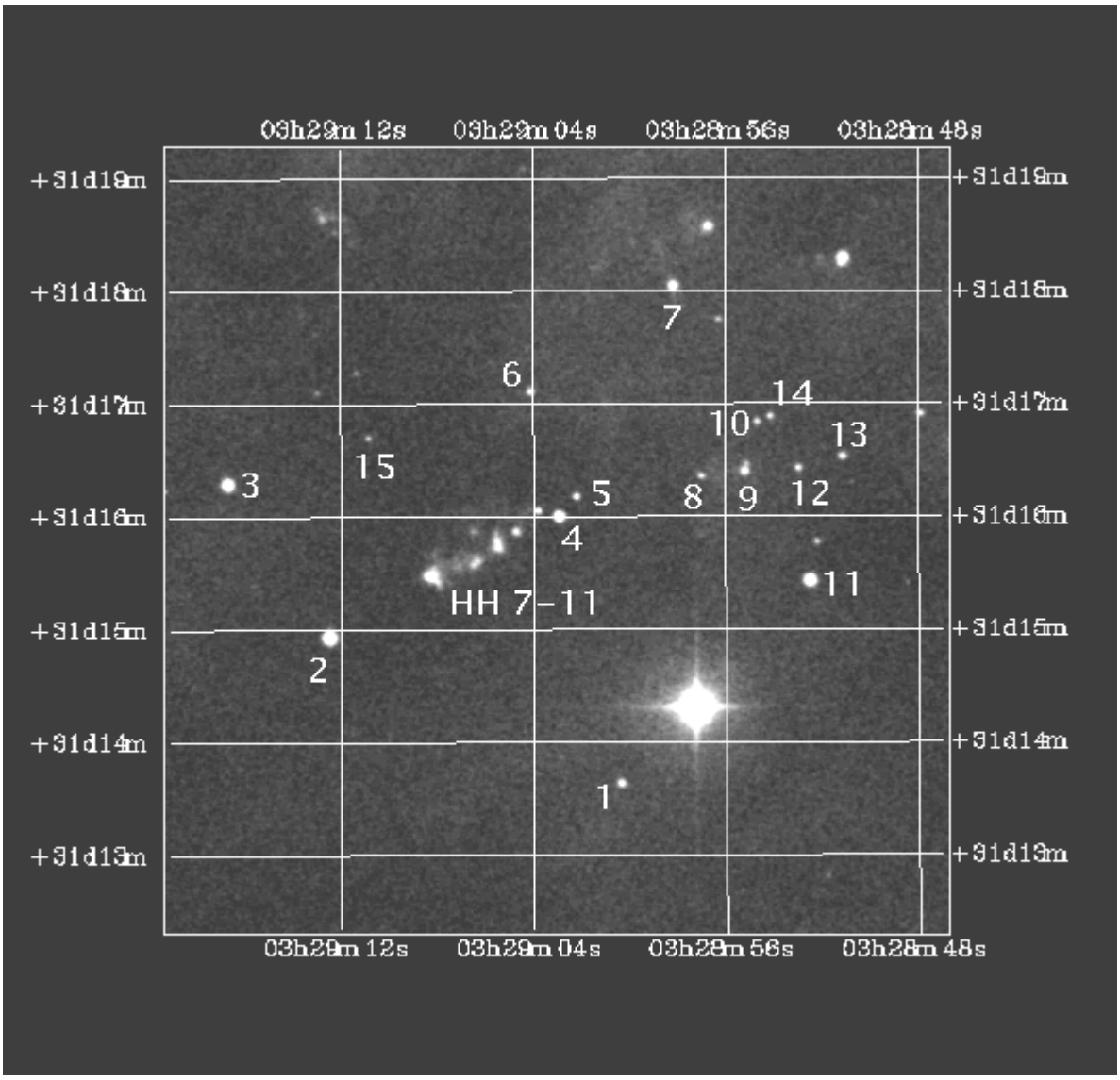

FIG. 1.—Reference stars for the HH 7–11 outflow in the DSS second-generation image, J2000.0 coordinates and field of view 7′

which at a distance of 330 pc correspond to a range of tangential velocities of ~26–73 km s^{-1} (Table 2). Except for HH 9, which has large uncertainties and may be almost stationary, the other objects are moving away from SVS 13, the driving source (Fig. 4), following its characteristic arc-shaped morphology. Overall, these motions are not that different from those presented by Herbig & Jones (1983) in their Figure 4. The total velocities (Table 3) can be estimated using the published radial velocities (Solf & Böhm 1987), with the largest value, ~185 km s^{-1}, for HH 11, the knot closer to the SVS 13 source. HH 9 has no published radial velocity, so a lower limit is set by its proper motion.

The DSS proper motions are 5–14 times *lower* than those measured using molecular hydrogen 2.12 μm images

TABLE 2

HH 7–11 AND CEPHEUS E (HH 377) PROPER MOTIONS

Object	PM_x (arcsec yr^{-1})	PM_y (arcsec yr^{-1})	PM_{tot} (arcsec yr^{-1})	P.A. (deg)	V_{tan}[a] (km s^{-1})
HH 7	0.022 ± 0.014	−0.007 ± 0.003	0.024 ± 0.014	108 ± 10	38 ± 23
HH 8	0.008 ± 0.001	−0.017 ± 0.005	0.019 ± 0.005	155 ± 21	30 ± 9
HH 9	−0.010 ± 0.006	0.011 ± 0.006	0.015 ± 0.009	318 ± 31	26 ± 15
HH 10	0.010 ± 0.005	−0.019 ± 0.008	0.022 ± 0.010	152 ± 50	36 ± 14
HH 11	0.039 ± 0.005	−0.020 ± 0.006	0.044 ± 0.007	117 ± 6	73 ± 12
HH 377.....	−0.013 ± 0.004	−0.028 ± 0.006	0.031 ± 0.004	206 ± 8	107 ± 14

[a] For distances d(HH 7–11) = 330 pc and d(Cep E) = 730 pc.

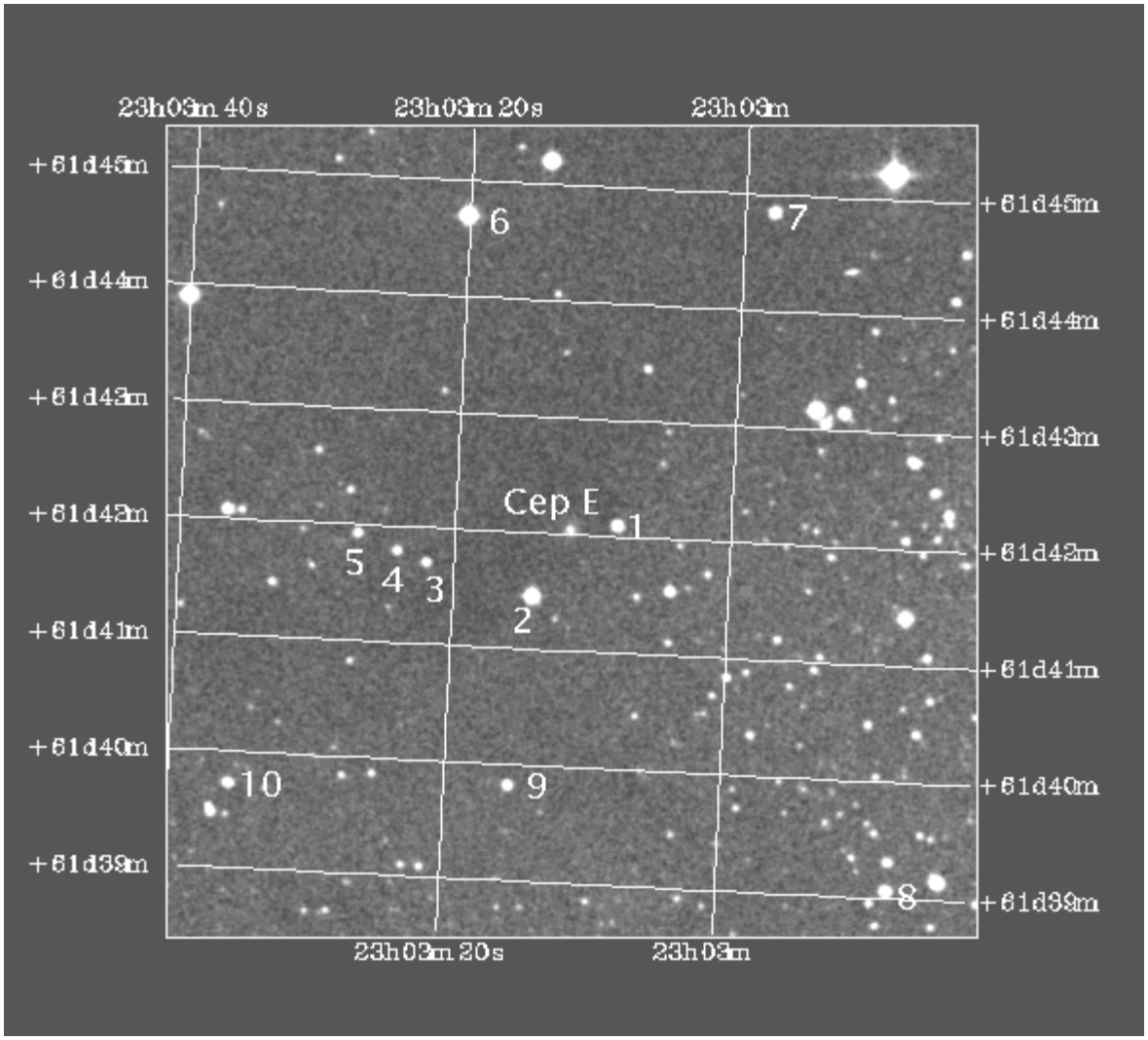

FIG. 2.—Same as Fig. 1, but for Cep E (HH 377). HH 377 lies between reference stars 1 and 2.

(Chrysostomou et al. 2000), for example, compared with that of HH 7, 0.″41 yr^{-1} in H_2 with the value 0.″024 yr^{-1} (but see below). Needless to say, if the atomic or ionic gas shares a similar motion with the H_2 gas, then it would be very easy to detect such large shifts in the optical images. We do not believe that this difference is real. We trust the optical results more than those from H_2 because of the longer time span (nearly 37 yr compared with 4–5 yr) and the larger number of well-selected and measured reference stars. These two ingredients are necessary to avoid systematic offsets, magnifications, and rotations that could bias the results in an unexpected fashion.

Although the shifts measured in the CCD [S II] images are consistent with those "predicted" by the DSS proper motions, there are some differences in detail, particularly for HH 7 and HH 10, as shown by the fits (*dotted line*) to their

TABLE 3

HH 7–11 AND CEPHEUS E (HH 377) VELOCITIES

Object	V_{rad}[a] (km s^{-1})	V_{tan} (km s^{-1})	V_{total} (km s^{-1})	γ[b] (deg)
HH 7	-51 ± 20	38 ± 23	63 ± 30	-53 ± 20
HH 8	-57 ± 20	30 ± 9	64 ± 15	-62 ± 13
HH 9	...	26 ± 15	...	...
HH 10	-35 ± 20	36 ± 14	50 ± 24	-44 ± 19
HH 11	-175 ± 20	73 ± 12	190 ± 19	-67 ± 6
HH 377.....	-70 ± 10	107 ± 14	128 ± 12	-33 ± 5

[a] From Solf & Böhm 1987 for HH 7, 8, 10, and 11 and from Ayala et al. 2000 for HH 337.

[b] From $\gamma = \tan^{-1}(V_{rad}/V_{tan})$.

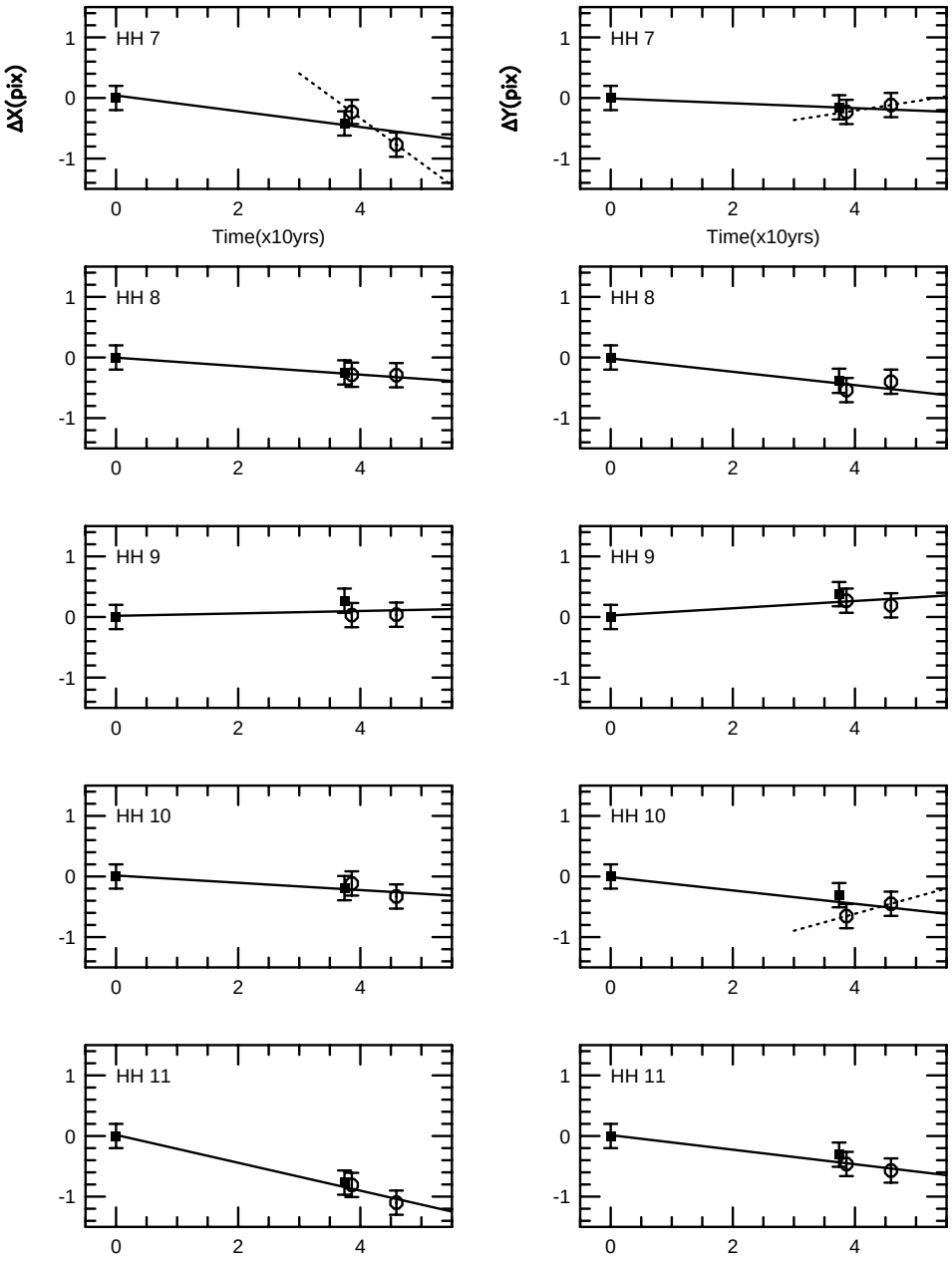

FIG. 3.—Difference in pixels in X-direction (*left*) and Y-direction (*right*) for the HH 7–11 images as a function of time (years). The squares correspond to the DSS measurements, while the circles correspond to those from [S II].

measurements (*circles*) in Figure 3. The proper motions for HH 7 based on the CCD [S II] images are $PM_x = -0\farcs12 \pm 0\farcs02$ yr^{-1} and $PM_y = 0\farcs08 \pm 0\farcs02$ yr^{-1}, which correspond to velocities of $V_x = 190 \pm 20$ km s^{-1} and $V_y = 130 \pm 20$ km s^{-1} for a distance of 330 pc. The tangential velocity derived from them is $V_{\rm tan} = 230 \pm 28$ km s^{-1} with position angle P.A. $= 56° \pm 7°$. This velocity is 5 times faster than the mean motion obtained from the DSS plates, but it is a bit misleading, since it is based *only* on the bow shock, without the Mach disk (which does not display a shift at all), and it is biased by the lower angular resolution of the 1993 image. But even if this estimate is correct, it is still a factor of 2 less than that obtained for HH 7A in H_2 of 450 ± 44 km s^{-1} by Chrysostomou et al. (2000), which assumes a distance of 220 pc. The case of HH 10 is less dramatic but shows the difficulty of using only two epochs separated by a relatively short period of time, since its shift in the Y-direction has a positive slope (Fig 3, *circles*). This means going from $PM_y = -0\farcs019 \pm 0\farcs008$ yr^{-1} to $PM_y = 0\farcs015 \pm 0\farcs02$ yr^{-1}, with a change of position angle of nearly 80°; the total tangential velocity is essentially the same as before.

Astrophysically, there are at least two reasons that indicate that the smaller proper motions are more appropriate; one is the luminosity of the source and the other is the low excitation of the objects. The recent interferometric maps of the HH 7–11 outflow (Bachiller et al. 2000), as well as the near-infrared NICMOS images (Noriega-Crespo, Cotera, & Young 2000), have confirmed that a jet arises from SVS 13 and that the molecular CO gas follows the path of the HH 7–11 optical knots, so there is little doubt that SVS 13 is the outflow source. SVS 13 is a relatively low mass young stellar

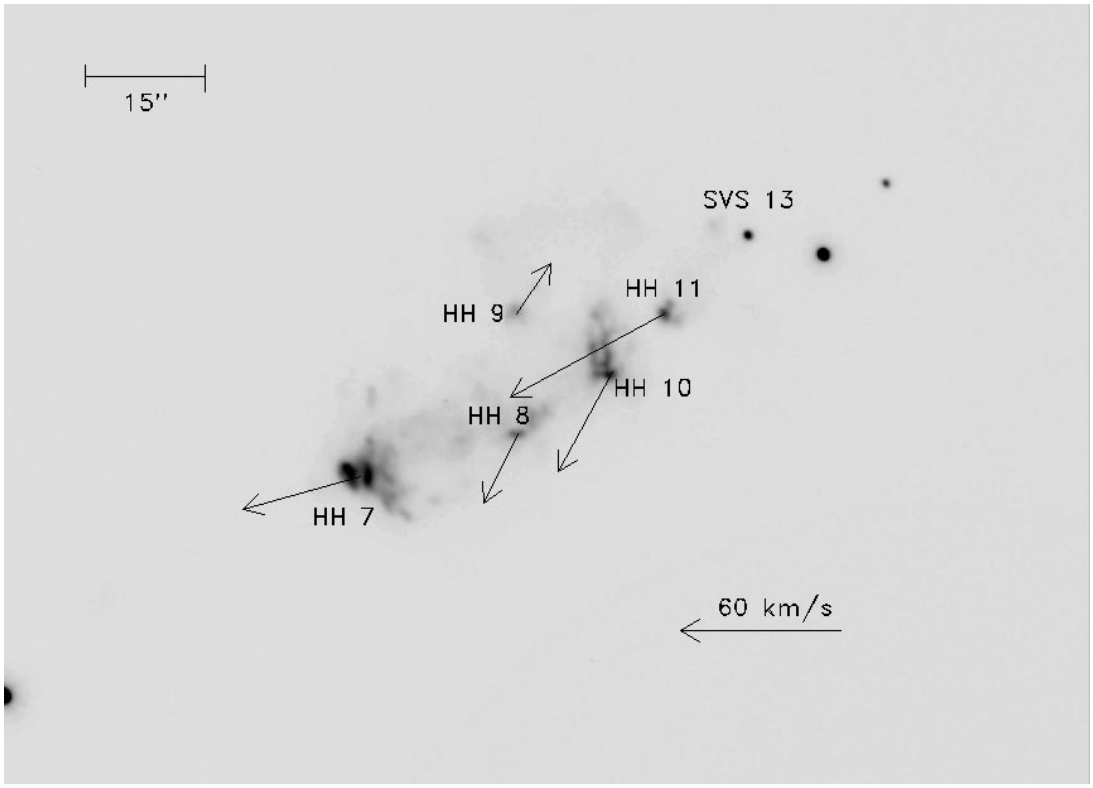

FIG. 4.—Graphic display of the tangential velocities of HH 7–11, based on the proper-motion measurements

object, with a bolometric luminosity of $\sim 85\ L_{\odot}$ (Molinari, Liseau, & Lorenzetti 1993), and so we do not expect outrageously high outflow velocities as seen in intermediate or high protostellar mass objects such as HH 80–81, for which flow velocities of ~ 600–$1400\ \mathrm{km\ s^{-1}}$ have been measured (Martí, Rodríguez, & Reipurth 1993), or ZCMa, with velocity $\geq 600\ \mathrm{km\ s^{-1}}$ (Poetzel, Mundt, & Ray 1989) and luminosities of 2×10^4 and $3500\ L_{\odot}$ (Martí et al. 1993; Hartmann et al. 1989). The other indicators are the shock velocities themselves, since at least at first approximation we expect high shock velocities for high flow velocities at the leading working surface. Again, this is what is observed in systems such as HH 1/2 or HH 80/81, where the [O III] emission confirms their higher excitation and shocks are higher than $100\ \mathrm{km\ s^{-1}}$. We do not see such high excitation in HH 7–11. The shock velocities obtained from the optical spectra for HH 7–11 are $\sim 40\ \mathrm{km\ s^{-1}}$ (Solf & Böhm 1987). The *Infrared Space Observatory* observations in the mid- to far-infrared also set a limit of ~ 40–$50\ \mathrm{km\ s^{-1}}$ for the shock velocities of both outflow lobes (Molinari et al. 2000), in agreement with the value derived using optical spectroscopic observations and consistent with the low-excitation nature of these objects.

Finally, the optical and H_2 measurements are really sampling different gases in the case of HH 7–11, and this is quite apparent from the superposition of 2.12 μm and [S II] emission. The extreme example corresponds to HH 11, which appears as a bullet even in the high angular resolution Wide Field Planetary Camera 2 images (Noriega-Crespo et al. 2000), while the H_2 emission is fuzzy, wide open, and a few arcseconds downstream, as one would expect from emission arising at the wings of a bow shock.

4.2. *Cep E = HH 377*

For HH 377, we proceed as with HH 7–11; we use the DSS plates to determine the mean proper motions, and then we analyze the shifts measured in the CCD images with the predicted values. The case for HH 377 is more simple

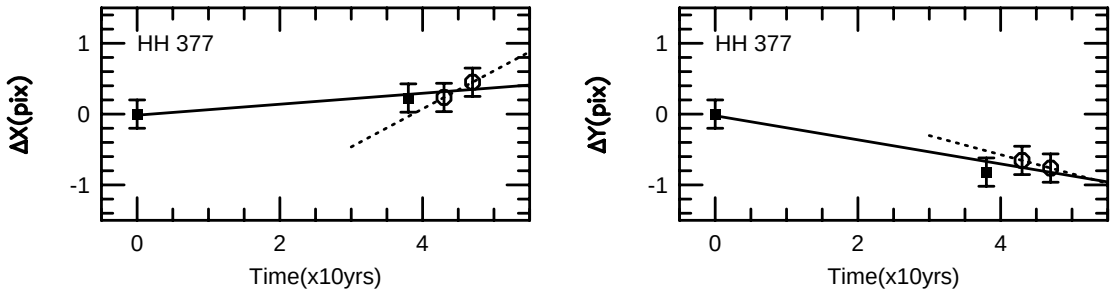

FIG. 5.—Same as Fig. 3, but for the Cep E (HH 377) images

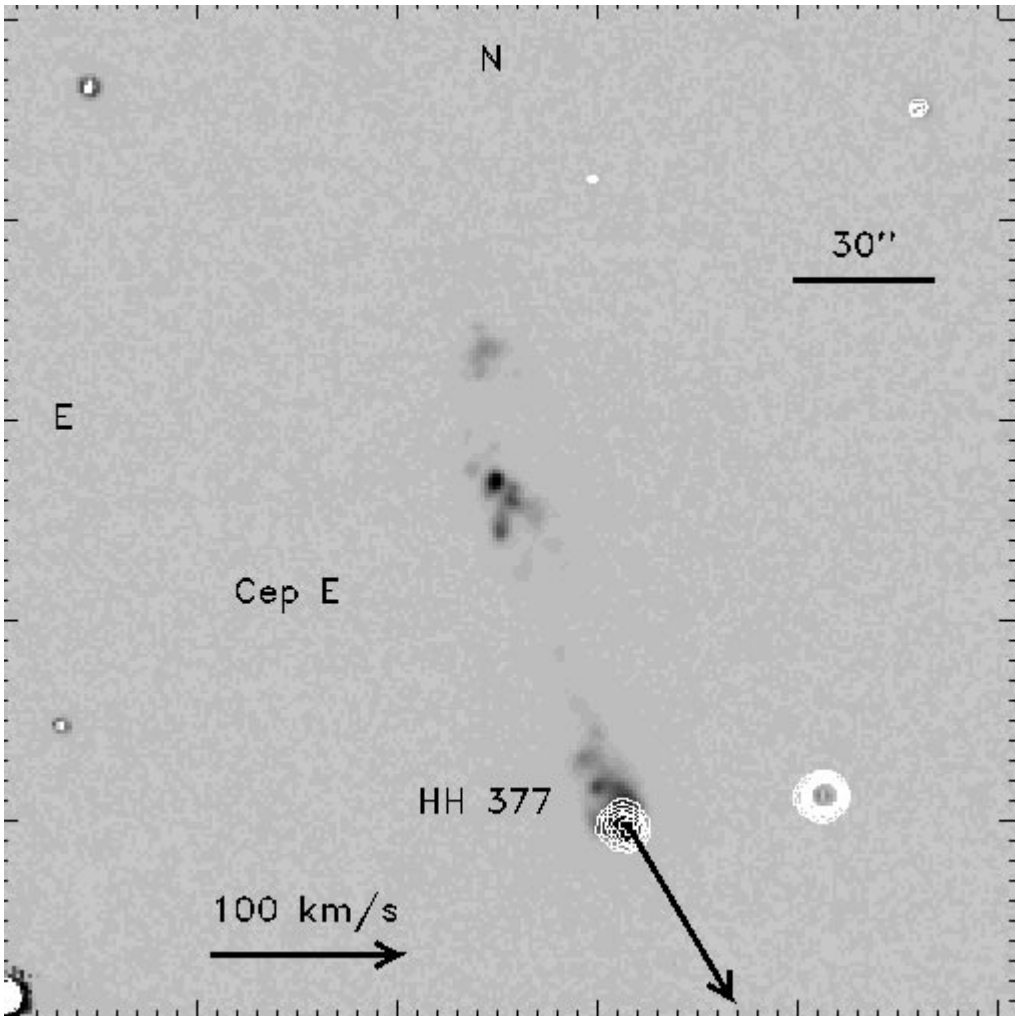

FIG. 6.—Same as Fig. 4, but for Cep E (HH 377)

than that for HH 7–11, since we are dealing with a single optical knot. Our measurements indicate that HH 377 is moving away from the IRAS 23011+6126 source (P.A. = 206° ± 8°) with a proper motion of 0.″031 ± 0.″004 yr^{-1} (Table 2; Fig. 5), which at a distance of 730 pc translates into a tangential velocity of ∼107 km s^{-1} (Fig. 6). The CCD measurements are consistent with their predicted values, although they could be higher, as indicated by the fit (*dotted line*) to the circles in Figure 5, i.e., $PM_x = -0.''068 \pm 0.''03$ yr^{-1} and $PM_y = -0.''077 \pm 0.''03$ yr^{-1}. This corresponds to $V_{tan} = 230 \pm 98$ km s^{-1} and P.A. = 220° ± 20°. We can estimate the flow velocity of Cep E by combining the proper motions and the radial velocity of HH 377. Thus, if we take the DSS mean proper motion and a mean radial velocity of about −70 km s^{-1} obtained from Hα, [S II] λλ6717/31, and [O I] λλ6300/63 emission lines (Ayala et al. 2000), we find a total velocity of ∼130 km s^{-1}. This flow velocity is quite similar to the 125 km s^{-1} obtained from the radio measurements of the ^{12}CO (2–1) molecular gas emission (Eislöffel et al. 1996) for the blue wing of the outflow.

For Cep E (HH 377), the shock velocities range from ∼15 to 35 km s^{-1}, based on optical and near-, mid-, and far-infrared spectroscopic observations (Ladd & Hodapp 1997; Ayala et al. 2000; Moro-Martín et al. 2001). The source itself, IRAS 23011+6126, a Class 0/I protostellar object, has a bolometric luminosity of 30 $L_\odot$; i.e., it is a low-mass young stellar object (Moro-Martín et al. 2001). So the power of the source and the magnitude of the flow and shock velocities are in agreement.

5. CONCLUSIONS

We have obtained the proper motions of two semi-embedded young stellar outflows, HH 7–11 and HH 377 (Cep E) by using optical images in [S II] and DSS plates epoch I and II. The HH 7–11 system has proper motions comparable in magnitude and direction to those previously obtained by Herbig & Jones (1983) but almost a factor of 10 smaller than those measured for the molecular hydrogen gas using H_2 2.12 μm near-infrared images.

Astrophysically it is difficult to see why there should be such a large discrepancy, and so we have argued in favor of the optical measurements based on a longer time baseline and a more accurate reference frame between the images at different epochs. If the optical measurements are correct, then this questions theoretical scenarios based on speeds exceeding 400 km s^{-1} for HH 7. Presently, however, we cannot rule out ideas that explain the observed excitation in HH 7/11 as the result of a fast jet propagating through a stationary medium that contains several dense clumps or structures (Chrysostomou et al. 2000). In this context it is interesting to note that HH 9, given its proper motion, may not be part of the HH 7–11 outflow, although certainly it is

a shock-excited condensation. We should point out, however, that ASR 57, another shock-excited clump $\sim 90''$ southeast from HH 7, seems to be related to the HH 7–11 outflow (Aspin et al. 1994) and might be the outcome of a previous major ejection event from SVS 13; if so, we are not necessarily dealing with a stationary medium. The case for HH 377 (Cep E) is more simple, and its proper motion is quite consistent with other velocity indicators, e.g., the ^{12}CO (2–1) outflow velocity wings, and with the overall bipolar morphology driven by IRAS 23011 + 6126.

We thank S. Curiel for making available to us his 1996 HH 7–11 optical images, A. Moro-Martin for her careful reading of the manuscript, and, last but not least, the referee, Jochen Eislöffel, for his insightful comments. The Digitized Sky Surveys were produced at the Space Telescope Science Institute under US government grant NAGW-2166. The images of these surveys are based on photographic data obtained using the Oschin Schmidt Telescope on Palomar Mountain and the UK Schmidt Telescope. The plates were processed into the present compressed digital form with the permission of these institutions. The National Geographic Society–Palomar Observatory Sky Atlas (DSS-I) and the Second Palomar Observatory Sky Survey (DSS-II) were produced by the California Institute of Technology.

REFERENCES

Aspin, C., Sandell, G., & Russell, A. P. G. 1994, A&AS, 106, 165
Ayala, S., Noriega-Crespo, A., Garnavich, P. M., Curiel, S., Raga, A. C., Böhm, K.-H., & Raymond, J. 2000, AJ, 120, 909
Bachiller, R., Gueth, F., Gilloteau, S., Tafalla, M., & Dutrey, A. 2000, A&A, 362, L33
Burrows, C. J., et al. 1996, ApJ, 473, 437
Chrysostomou, A., Hobson, J., Davis, C. J., Smith, M. D., & Berndsen, A. 2000, MNRAS, 314, 229
Curiel, S., Raga, A., Raymond, J., Noriega-Crespo, A., & Cantó, J. 1997, AJ, 114, 2736
Devine, D., Bally, J., Reipurth, B., & Heathcote, S. 1997, AJ, 114, 2095
Devine, D., Reipurth, B., & Bally, J. 1997, in Low Mass Star Formation: From Infall to Outflow, ed. F. Malbet & A. Castets (Grenoble: Obs. Grenoble), 91
Eislöffel, J., & Mundt, R. 1992, A&A, 263, 292
———. 1994, A&A, 284, 530
Eislöffel, J., Mundt, R., & Böhm, K.-H. 1994, AJ, 108, 1042
Eislöffel, J., Smith, M. D., Davis, C. J., & Ray, T. P. 1996, AJ, 112, 2086
Hartigan, P., Morse, J., Reipurth, B., Heathcote, S., & Bally, J. 2001, ApJ, 559, L157
Hartmann, L., Kenyon, S. J., Hewett, R., Edwards, S., Strom, K. M., Strom, S. E., & Stauffer, J. R. 1989, ApJ, 338, 1001
Heathcote, S., & Reipurth, B. 1992, AJ, 104, 2193
Herbig, G. H., & Jones, B. F. 1981, AJ, 86, 1232
———. 1983, AJ, 88, 1040
Ladd, E. F., & Hodapp, K.-W. 1997, ApJ, 474, 749
Lee, J.-K., & Burton, M. G. 2000, MNRAS, 315, 11
López, R., et al. 1998, AJ, 116, 845
Martí, J., Rodríguez, L. F., & Reipurth, B. 1993, ApJ, 416, 208
———. 1998, ApJ, 502, 337
Micono, M., Davis, C. J., Ray, T. P., Eislöffel, J., & Shetrone, M. D. 1998, ApJ, 494, L227
Molinari, S., Liseau, R., & Lorenzetti, D. 1993, A&AS, 101, 59
Molinari, S., et al. 2000, ApJ, 538, 698
Moro-Martín, A., Noriega-Crespo, A., Molinari, S., Testi, L., Cernicharo, J., & Sargent, A. 2001, ApJ, 555, 146
Noriega-Crespo, A. 1997, in IAU Symp. 182, Herbig-Haro Flows and the Birth of Stars, ed. B. Reipurth & C. Bertout (Dordrecht: Kluwer), 103
Noriega-Crespo, A., Cotera, A., & Young, E. 2000, BAAS, 197, No. 10.08
Noriega-Crespo, A., Garnavich, P. M., Curiel, S., Raga, A. C., & Ayala, S. 1997, ApJ, 486, L55
Poetzel, R., Mundt, R., & Ray, T. P. 1989, A&A, 224, L13
Pravdo, S. H., Rodríguez, L. F., Curiel, S., Cantó, J., Torrelles, J. M., Becker, R. H., & Sellgren, K. 1985, ApJ, 293, L35
Raines, S. N., et al. 2000, ApJ, 528, L115
Reipurth, B., Heathcote, S., Roth, M., Noriega-Crespo, A., & Raga, A. C. 1993, ApJ, 408, L49
Reipurth, B., Raga, A. C., & Heathcote, S. 1992, ApJ, 392, 145
———. 1996, A&A, 311, 989
Rodríguez, L. F., Ho, P. T. P., Torrelles, J. M., Curiel, S., & Cantó, J. 1990, ApJ, 352, 645
Solf, J., & Böhm, K.-H. 1987, AJ, 93, 1172
Strom, S. E., Vrba, F. J., & Strom, K. M. 1976, AJ, 81, 314